Observations and a Model of Undertow over the Inner Continental Shelf

Steven J. Lentz

Woods Hole Oceanographic Institution, Woods Hole, MA

Melanie Fewings

Woods Hole Oceanographic Institution, Woods Hole, MA

Peter Howd

USGS, St. Petersburg, FL

Janet Fredericks

Woods Hole Oceanographic Institution, Woods Hole, MA

Kent Hathaway

USACE CHL Field Research Facility, Kitty Hawk, NC

March 28, 2008;

revised and resubmitted to JPO

Corresponding author:

Steven J. Lentz

Woods Hole Oceanographic Institution, MS 21

Woods Hole, MA 02543

slentz@whoi.edu

1

Abstract

Onshore volume transport (Stokes drift) due to surface gravity waves propagating toward the beach is known to result in a compensating Eulerian offshore flow in the surfzone referred to as undertow. Observed offshore flows indicate wave-driven undertow extends well offshore of the surfzone, over the inner shelves of Martha's Vineyard, Massachusetts and North Carolina. Theoretical estimates of the wave-driven offshore transport from linear wave theory and observed wave characteristics account for 50% or more of the observed offshore transport variance in water depths between 5 m and 12 m, and reproduce the observed dependence on wave height and water depth.

During weak winds, wave-driven cross-shelf velocity profiles over the inner shelf have maximum offshore flow (1–6 cm s^{-1}) and vertical shear near the surface, and weak flow and shear in the lower half of the water column. The observed offshore flow profiles do not resemble the profiles observed within the surfzone, which are parabolic with maximum flow at mid-depth. Instead, the vertical structure is similar to the Stokes drift velocity profile but with the opposite direction. This vertical structure is consistent with a dynamical balance between the Coriolis force associated with the offshore flow and an along-shelf "Hasselmann wave stress" due to the influence of the Earth's rotation on surface gravity waves. The close agreement between the observed and modeled profiles provides compelling evidence for the importance of the Hasselmann wave stress in forcing oceanic flows. Summer profiles are more vertically sheared than either winter profiles or model profiles, for reasons that remain unclear.

1. Introduction

The inner shelf is the region between the surfzone and the mid continental shelf. The location and width of the inner shelf varies depending on wave heights, winds, stratification, and other processes but typically spans water depths from a few meters to a few tens of meters. The cross-shelf circulation over the inner shelf is important to a variety of interdisciplinary processes including coastal upwelling of nutrients, larval transport between the nearshore and the rest of the continental shelf, on-offshore sediment transport, and the dispersal of contaminants.

Studies of cross-shelf circulation over the inner shelf have focused on along-shelf wind forcing and how the wind-driven cross-shelf circulation decreases from the mid shelf toward the coast as the water depth decreases (Lentz 1994; Lentz et al. 2003; Kirincich et al. 2005). These studies have found that cross-shelf flows driven by along-shelf winds are substantially reduced over the inner shelf, particularly in the shallow water just outside the surfzone. In the surfzone, the circulation is predominantly driven by breaking surface gravity waves. There is often an offshore flow (undertow) within the surfzone (Haines and Sallenger 1994; Garcez Faria et al. 2000; Reniers et al. 2004) that compensates for the onshore (Stokes) transport due to the waves (Stokes 1847). While a recent observational study has indicated the importance of wave forcing to the depth-averaged momentum balances over the inner shelf (Lentz et al. 1999), there have not been any observational studies that examine wave-driven cross-shelf circulations over the inner shelf.

Observations are presented here of wave-driven offshore flows (undertow) extending well seaward of the surfzone into water depths of 5–17 m, over the inner shelves of Martha's Vineyard, Massachusetts and North Carolina. In both cases, undertow is the dominant component of the depth-averaged cross-shelf circulation over time scales of days to weeks onshore of the 15-m isobath. A simple model is developed (section 2) to provide a dynamical interpretation of the observed undertow profiles. When wind stresses are weak, mean cross-shelf velocity profiles over the inner shelf (offshore of the surfzone) do not resemble the

parabolic profiles observed in the surfzone (Fig. 1a) (Haines and Sallenger 1994; Garcez Faria et al. 2000; Reniers et al. 2004). Instead, the profiles have maximum offshore flow near the surface, decreasing toward the bottom (Fig. 1b), consistent with a dynamical balance between the Coriolis force and the Hasselmann (or Stokes-Coriolis) wave stress (Hasselmann 1970) due to the influence of the Earth's rotation on surface gravity waves. The response of the cross-shelf flow at the Martha's Vineyard site to wind forcing and combined wind and wave forcing is presented in a companion paper (Fewings et al. 2008).

2. Undertow model description

There have been numerous theoretical and laboratory studies of undertow in the vicinity of the surfzone (*e.g.*, Nadaoka and Kondoh 1982; Svendsen 1984; Stive and Wind 1986; Putrevu and Svendsen 1993; Ting and Kirby 1994; Govender et al. 2002). To investigate the dynamics of undertow outside the surfzone, a simple model is developed that includes the influence of the Earth's rotation on both the wave forcing and the wave-driven circulation. The model builds on the one-dimensional (no horizontal variations) model of Xu and Bowen (1994) by allowing for cross-shelf variations, while still assuming no along-shelf variations. The key additions to the Xu and Bowen model are the inclusion of a coastal boundary condition implying no net cross-shelf transport (section 2a), and the inclusion of a cross-shelf pressure gradient and a momentum flux divergence due to shoaling surface gravity waves in the cross-shelf momentum budget (section 2b).

a. Undertow transport: Volume conservation

Assuming a steady state, no along-shelf variations in the flow such as rip currents, and no cross-shelf transport at the coast, integrating the continuity equation from the free surface ($z = \eta + \tilde{\eta}$) to the bottom ($z = -h$) yields

$$\overline{\int_{-h}^{\eta+\tilde{\eta}} (u + \tilde{u})\, dz} = \overline{\int_{\eta}^{\tilde{\eta}} \tilde{u}\, dz} + \int_{-h}^{\eta} \overline{(u + \tilde{u})}\, dz = Q_w + \int_{-h}^{\eta} u\, dz = 0, \qquad (1)$$

where u is the cross-shelf velocity (positive for offshore flow) and an overbar indicates an

4

average over time scales long compared to the wave period. Variables have been decomposed into surface wave variations, $\tilde{\eta}$ and $\tilde{u}$, and average values over a time long compared to the wave period, η and u. Additionally, linear surface gravity waves are assumed so $\overline{\tilde{u}} = 0$ below the wave troughs and Q_w is the onshore (Stokes) transport above the wave troughs (Stokes 1847). For linear surface gravity waves, the Stokes transport is

$$Q_w \approx \frac{gH_{sig}^2}{16c} \cos(\theta_w), \tag{2}$$

where g is gravitational acceleration, H_{sig} is the significant wave height (defined as four times the standard deviation of $\tilde{\eta}$), c is the phase speed of the waves, and θ_w is the wave direction relative to offshore ($\theta_w = 180°$ for waves propagating directly onshore) (e.g., LeBlond and Mysak 1978; Mei 1983). The Stokes transport is concentrated above the wave troughs in an Eulerian frame or is the vertically-distributed Stokes drift in a Lagrangian frame. The compensating depth-averaged offshore flow, assuming $\eta << h$, is

$$u_w \approx \frac{1}{h} \int_{-h}^{\eta} u \ dz = -\frac{Q_w}{h} = -\frac{gh}{16c} \left(\frac{H_{sig}}{h}\right)^2 \cos(\theta_w), \tag{3}$$

positive for offshore flow.

Within the surfzone, while "mean" (average over many wave periods) offshore flows have often been observed at single depths (e.g., Wright et al. 1982; Masselink and Black 1995), only a few studies have obtained velocity profiles to accurately estimate offshore transport and test (3) (Garcez Faria et al. 2000; Reniers et al. 2004). Using current profiles measured from a sled system that sampled different locations within and just seaward of the surfzone (water depths 1–4 m) near Duck, North Carolina, Garcez Faria et al. (2000) found reasonable agreement between $-Q_w$ and the observed offshore transport except on the shoreward side of a shore-parallel sandbar. Inclusion of an estimate of the onshore transport due to wave rollers in the surfzone improved the agreement. Using a similar sled system at the same site, Reniers et al. (2004) found larger differences between $-Q_w$ plus the wave-roller transport and the observed offshore transport, which they attributed to along-shelf variability.

The contribution of undertow to the cross-shelf transport over the inner shelf, offshore of the surfzone (defined here as $h > 2H_{sig}$), is not known. Assuming shallow-water waves

5

$(c \approx \sqrt{gh})$ propagating onshore ($\theta_w = 180°$) with $H_{sig} = 2$ m, the depth-averaged offshore flow estimated from (3) is 2.5 cm s^{-1} in 10 m of water. This is comparable to observed depth-averaged cross-shelf flows (below the wave troughs) over inner shelves (*e.g.*, Lentz and Winant 1986; Lee et al. 1989; Lentz et al. 1999; Kirincich et al. 2005), suggesting wave forced cross-shelf flows may be important over the inner shelf.

b. Momentum balances

Estimates of the offshore transport using (3) are based only on volume conservation, the assumption of no along-shelf variations in the flow, and the estimated wave-driven onshore transport (2). Consequently, while (3) may be used to infer whether observed offshore transports are forced by surface waves, it does not provide much insight into the underlying dynamics. The structure of the velocity profiles does provide insight into the dynamics.

Assuming steady, linear dynamics for the wave-averaged flow, with no along-shelf variations, constant density, and no wave breaking, the momentum balances are

$$-fv = -g\eta_x - [\overline{(\tilde{u}^2)}_x + \overline{(\tilde{u}\tilde{w})}_z] + (Au_z)_z, \tag{4}$$

$$fu = -[\overline{(\tilde{u}\tilde{v})}_x + \overline{(\tilde{v}\tilde{w})}_z] + (Av_z)_z. \tag{5}$$

where f is the Coriolis frequency, v and w are along-shelf and vertical velocities, x and z subscripts indicate partial derivatives, and A is an eddy viscosity used to represent the turbulent Reynolds stresses. To isolate different dynamical balances, the wave forcing terms in square brackets in (4) and (5) are decomposed into three separate contributions: F^{ws} is the momentum flux contribution from $\overline{(\tilde{u}^2)}_x + \overline{(\tilde{u}\tilde{w})}_z$ due to wave shoaling (without friction or rotation); $\boldsymbol{\tau}^{wb}$ is the wave stress from $(\overline{(\tilde{u}\tilde{w})}_z, \overline{(\tilde{v}\tilde{w})}_z)$ due to bottom friction acting on the waves; and the Hasselmann wave stress $\boldsymbol{\tau}^{wH}$ associated with the modification of the waves by the Earth's rotation is $(\overline{(\tilde{v}\tilde{w})}_z, \overline{(\tilde{u}\tilde{w})}_z)$. Each of these contributions is discussed in turn below.

6

As surface gravity waves propagate into shallower water (shoal) without breaking there is a divergence in the wave-forced momentum flux (Longuet-Higgins and Stewart 1964). Outside the surfzone, this momentum flux divergence is oriented cross-shelf. In the following, the momentum flux divergence due to wave shoaling F^{ws} is not determined explicitly from the wave evolution. Instead, F^{ws} is assumed to be independent of depth and combined with the unknown cross-shelf pressure gradient $g\eta_x$, as in Garcez Faria et al. (2000). As described below, the value of $(-g\eta_x - F^{ws})$ is found that satisfies (1).

Bottom friction acting on the waves causes $\tilde{u}$ and $\tilde{w}$ to be slightly in phase resulting in a wave stress $\overline{(\tilde{u}\tilde{w})}$ that causes near-bottom wave streaming in the direction of wave propagation (Longuet-Higgins 1953). Following Xu and Bowen (1994), the cross-shelf component of the depth-dependent wave stress divergence concentrated near the bottom is

$$\tau_z^{wbx} = -\rho\overline{(\tilde{u}\tilde{w})}_z = \frac{H_{sig}^2\omega^2 k}{16\sinh^2(kh)}[(-\beta z'\sin(\beta z') + \beta z'\cos(\beta z') - \cos(\beta z'))e^{-\beta z'} - e^{-2\beta z'}], \quad (6)$$

where ω is the wave frequency, k is the cross-shelf wave number, $\beta = \sqrt{\omega/2A}$ and $z' = h - z$ is height above the bottom.

Hasselmann (1970) showed that the Coriolis force acting on surface wave velocities would induce a small (order $f/\omega \approx 10^{-4}$, where $\omega \approx 1$ s^{-1} and $f \approx 10^{-4}$ s^{-1}) along-crest wave velocity $\tilde{v}$ that is in phase with the vertical wave velocity $\tilde{w}$. Though $\tilde{v}$ is small, the resulting wave stress $\tau^{wH} = -\rho_\circ\overline{(\tilde{v}\tilde{w})}$ (referred to as the Hasselmann wave stress or Stokes-Coriolis forcing; the former will be used here) can be substantial relative to the wind stress (*e.g.*, McWilliams and Restrepo 1999). It has been suggested that this is a potentially important forcing mechanism for both shelf flows (*e.g.*, Xu and Bowen 1994; Newberger and Allen 2007b) and the open ocean circulation (*e.g.*, Hasselmann 1970; McWilliams and Restrepo 1999; Ardhuin et al. 2004; Polton et al. 2005). For onshore propagating waves ($\theta_w = 180°$), the vertical divergence in the along-crest (Hasselmann) wave stress is

$$\tau_z^{wHx} = -\rho_\circ\frac{H_{sig}^2 f\omega k}{16}\frac{\cosh(2k[z+h])}{\sinh^2(kh)} = -\rho_\circ f u_{st} \quad (7)$$

where

$$u_{st} = \frac{H_{sig}^2 \omega k}{16} \frac{\cosh(2k[z+h])}{\sinh^2(kh)} \tag{8}$$

is the Stokes velocity (*e.g.*, Stokes 1847; LeBlond and Mysak 1978; Mei 1983). Recent studies have generalized the Hasselmann wave stress concept to include spatially-varying wave and wave-averaged flow fields (*e.g.*, McWilliams et al. 2004; Ardhuin et al. 2004; Smith 2006).

Incorporating the wave-forcing terms described above, the momentum balances are

$$-fv = fv_{st} - g\eta_x - F^{ws} + \tau_z^{wbx}/\rho_\circ + (Au_z)_z, \tag{9}$$

$$fu = -fu_{st} + \tau_z^{wby}/\rho_\circ + (Av_z)_z, \tag{10}$$

where τ_z^{wby} in (10) and fv_{st} in (9) account for waves propagating onshore at an angle to the isobaths ($\theta_w \neq 180°$). Assuming no wind stress ($\boldsymbol{\tau}^s = 0$) and no wave breaking over the inner shelf, the surface boundary condition is a wave-driven surface stress vector $\boldsymbol{\tau}^{ws}$ at the outer edge of the thin viscous wave boundary layer (Longuet-Higgins 1953; Xu and Bowen 1994):

$$\frac{\boldsymbol{\tau}^{ws}}{\rho_\circ} = A\mathbf{u}_z = \frac{AH_{sig}^2}{4}\omega\mathbf{k}|\mathbf{k}|\coth(|\mathbf{k}|h) \text{ at } z \approx 0, \tag{11}$$

where $\mathbf{k}$ is the wave-number vector, and the bottom boundary condition is no flow at the bottom: $\mathbf{u} = (u, v) = 0$ at $z = -h$.

The model consists of three equations, (1), (9), and (10) and three unknowns, u, v, and η_x or in the present application $(g\eta_x + F^{ws})$. Given the wave forcing and assuming a constant eddy viscosity A, the equations are solved semi-analytically for u and v as a linear superposition of flows driven by the surface wave stress (11), the bottom wave stress (6), the Hasselmann wave stress (7), and the sum of the depth-independent pressure gradient and momentum flux due to wave shoaling $(g\eta_x + F^{ws})$. Analytic expressions for the response to the surface wave stress, bottom wave stress, and Hasselmann wave stress are given by Xu and Bowen (1994) and for a vertically uniform body force $g\eta_x + F^{ws}$ by Ekman (1905) (see also Winant 2006). The third unknown, $g\eta_x + F^{ws}$, is found by iteratively searching for the value that satisfies no net onshore volume transport, (1). The sea surface slope η_x may be determined

separately from the depth-averaged cross-shelf momentum balance given a model for the cross-shelf evolution of the waves to estimate the momentum flux due to wave shoaling (*e.g.*, Longuet-Higgins and Stewart 1964; Garcez Faria et al. 2000).

Equations (1), (9), and (10) were also solved numerically for more "realistic" eddy-viscosity profiles for unstratified flows in which the shape of the eddy-viscosity profile is prescribed, but the magnitude depends on the surface and bottom stresses (for details, see Lentz 1995). The numerical model results indicate the cross-shelf velocity profiles are not sensitive to the form of the eddy viscosity, although the along-shelf velocity profiles are sensitive to the eddy viscosity (Appendix A).

c. Modeled profiles

The contributions of the four forcing terms to the velocity profiles are illustrated in Fig. 2 for a case in which the eddy viscosity is small (see below; non-dimensionally $\delta^E/h << 1$, where $\delta^E = \sqrt{2A/f}$ is the Ekman boundary layer scale) and $\theta_w = 180°$. The depth-independent body force $\eta_x + F^{ws}$ forces a negative along-shelf flow that is vertically uniform except in the bottom boundary layer where the along-shelf flow decreases to zero and there is an offshore flow associated with Ekman veering (Ekman 1905). The vertically-distributed Hasselmann wave stress forces an offshore flow throughout the water column with small along-shelf flows near the surface and bottom. The near-bottom wave stress forces an onshore near-bottom flow with some veering and the surface stress forces an onshore near-surface flow with some veering. The superposition of these four contributions results in an offshore flow, primarily due to the Hasselman wave stress, that increases toward the surface and an along-shelf flow that is maximum at mid-depth and decreases toward the surface and bottom.

The structure of the model velocity profiles depends on the magnitude of the eddy viscosity or δ^E/h (Fig. 3). If the eddy viscosity is large ($A > 10^{-3}$ m² s⁻¹) so that the boundary layers span the water column ($\delta^E/h > 0.4$), the cross-shelf velocity profiles are parabolic with maximum offshore flow near mid-depth and the along-shelf velocity is small compared to the cross-shelf flow. If the eddy viscosity is small ($A < 10^{-3}$ m² s⁻¹ or $\delta^E/h < 0.4$), the

cross-shelf velocity is largest near the surface and decreases with depth, and the along-shelf velocity is similar in magnitude to the cross-shelf velocity. The dynamics in these two limits can be understood in the context of (9) and (10).

For large eddy viscosity ($\delta^E/h >> 1$), the Coriolis (fu, fv) and Hasselmann wave stress (fu_{st}, fv_{st}) terms can be neglected and the cross-shelf velocity profile is determined by (9). Equation (9) reduces to a balance between the depth-independent body force ($-g\eta_x - F^{ws}$) and the vertical gradient of the turbulent stress,

$$0 = -g\eta_x - F^{ws} + (Au_z)_z, \tag{12}$$

where the near-bottom wave stress is incorporated into the bottom boundary condition as an onshore wave streaming velocity at the bottom (Longuet-Higgins 1953). Assuming no net cross-shelf transport (3), an onshore surface wave stress (11), and either no flow at the bottom or an onshore wave streaming in the wave bottom boundary layer (*e.g.*, Longuet-Higgins 1953; Stive and Wind 1986), (12) yields a quadratic cross-shelf velocity profile with maximum offshore flow at mid-depth, decreasing toward both the surface and bottom (Fig. 3, $A \geq 10^{-3}$ m^2 s^{-1} curves). Neglecting the Coriolis (fu) and Hasselmann wave stress (fu_{st}) terms in (10) and noting there is no along-shelf surface stress implies both the along-shelf bottom stress and the along-shelf flow are zero. This follows from there being no along-shelf forcing and no Coriolis terms coupling the cross-shelf and along-shelf momentum balances.

Equation (12) is the momentum balance considered in surfzone studies of undertow, but with F^{ws} representing the onshore momentum flux divergence due to breaking waves rather than the shoaling of waves that are not breaking (*e.g.*, Svendsen 1984; Stive and Wind 1986; Putrevu and Svendsen 1993; Haines and Sallenger 1994; Garcez Faria et al. 2000; Reniers et al. 2004). In the surfzone, there is a shoreward surface stress associated with the breaking waves (*e.g.*, Stive and Wind 1986; Newberger and Allen 2007a) and there can also be an onshore mass flux due to wave rollers (Garcez Faria et al. 2000; Reniers et al. 2004). The few oceanographic field studies of undertow in the vicinity of the surfzone found parabolic offshore velocity profiles with maximum offshore flows either at mid depth (Haines and

Sallenger 1994) or near the bottom (Garcez Faria et al. 2000; Reniers et al. 2004) consistent with (12). A recent numerical modeling study that included an onshore surface stress due to breaking waves and wave rollers produced good agreement with observed current profiles within the surfzone (Newberger and Allen 2007b).

If the eddy viscosity is small, $A \leq 10^{-4}$ m^2 s^{-1} or $\delta^E/h << 1$, the turbulent stress terms can be neglected except in thin surface and bottom boundary layers (*e.g.,* Fig. 2). In this case, the cross-shelf velocity profile is determined by the Hasselmann wave stress since (10) reduces to

$$fu = -fu_{st}. \tag{13}$$

Thus, the cross-shelf velocity profile is equal in magnitude but opposite in direction to the Stokes velocity given by (8). This suggests the cross-shelf velocity profiles over the inner shelf may be quite different from the parabolic surfzone profiles if the turbulent stresses are small. If $\theta_w = 180°$, the corresponding interior along-shelf velocity is determined by the difference between the onshore momentum flux divergence due to wave shoaling and the cross-shelf pressure gradient.

3. Data sets and processing

To investigate undertow, current and wave observations from two locations are analyzed: the inner shelf south of Martha's Vineyard, near Cape Cod, Massachusetts and the inner shelf near Duck, North Carolina.

Observations have been collected for the last 6 years at the Martha's Vineyard Coastal Observatory (MVCO) including current and wave measurements from a bottom-mounted RDI 1200-kHz BroadBand Acoustic Doppler Current Profiler (ADCP) deployed 1.5 km offshore in 12 m of water. Twenty-minute averages of current profiles and surface-wave characteristics, including wave spectra and average wave direction as a function of frequency, for the period 1 June 2001 to 26 May 2006 were obtained from the MVCO website (http://www.whoi.edu/mvco). The ADCP has a sample rate of 2 Hz and 0.5-m vertical bins between 2.5 m and 10 m above the bottom. There are several gaps in the time series

lasting 1–4 months. Additionally, four periods of data when both the ADCP signal strength and the signal correlation are small (6 February - 17 April 2002, 22 February - 4 April 2004, 8 - 19 April 2005, and 2 February - 7 March 2006) were discarded because bin-to-bin velocity differences and wave characteristics are anomalous during these periods. Significant wave height H_{sig}, dominant wave period, and dominant wave direction θ_w were estimated from wave spectra of the ADCP current observations as described at the MVCO website.

Three additional mooring sites near MVCO have been instrumented for shorter periods of time as part of the ongoing Stratification, Wind, and Waves on the Inner shelf of Martha's Vineyard (SWWIM) study. SWWIM current profiles are from a 1200-kHz ADCP in 7-m water depth (0.4 km offshore) and two 600-kHz ADCPs in 17-m and 27-m water depth (3.8 km and 11.1 km offshore). The observations span 11 October 2006 - 17 August 2007 at the 7-m site; 11 October 2006 - 19 April 2007 and 21 May - 24 August 2007 at the 17-m site; and 7 December 2004 - 23 May 2005, 11-28 October 2006, and 21 May - 24 August 2007 at the 27-m site. The ADCP at the 7-m site recorded 6.7 or 9 minute burst averages of 1 sec samples every 20 minutes with 0.25-m bins. The ADCPs at the 17-m and 27-m sites recorded 5 minute burst averages of 1 sec samples every 20 minutes with 0.5-m bins. The ADCPs were also configured to estimate wave characteristics every 3 hours during the 2006-2007 deployments using the RDI wave software (Wavesmon version 2.02). Wave heights from the 12-m (MVCO node) and 27-m sites are highly correlated (0.98) with a regression slope of 1.02 suggesting little variation across the array. Consequently, the MVCO 12-m site wave observations are used for the 17-m and 27-m sites since wave measurements are not always available at these two sites. Wave height measurements at the 7-m site are used for that site because there is a complete time series and wave heights decrease substantially between the 12-m and 7-m sites during a few large wave events ($H_{sig} > 3.5$ m) when the 7-m site was in the surfzone ($H_{sig} > h/2$). Wind observations for both MVCO and SWWIM are primarily from a 10-m shore mast (12.5 m above mean sea level) with some data gaps filled using winds from a second site farther onshore (Fewings et al. 2008). All SWWIM time series were averaged and/or interpolated onto the MVCO time base with samples every 20 minutes.

Observations from the North Carolina inner shelf are from the 1997 SandyDuck field program conducted near the Army Corps of Engineers Field Research Facility (FRF). SandyDuck current profiles are from 6 upward-looking SonTek/YSI Acoustic Doppler Profilers (ADPs) (5.2–12.0 m depth) and one upward-looking RDI BroadBand 1200-kHz ADCP (12.7 m depth), deployed from 17 September to 10 November 1997. Six of the profilers were deployed on a cross-shelf transect in water depths of 5.2 m, 6.5 m, 7.7 m, 8.7 m, 12.0 m, and 12.7 m (0.3, 0.5, 0.6, 0.8, 1.2, and 1.5 km offshore). The seventh profiler was deployed in 6.5 m water (0.5 km offshore) about 100 m to the south. The ADP at 5.2 m depth was a 3000-kHz unit with 0.25-m bins, and the other ADPs were 1500-kHz units with 0.5-m bins. The ADPs recorded 3.5-minute mean velocities every 5 min. The ADCP at 12.7 m recorded 1-min mean velocities and had 0.5-m bins. The velocities from the ADCP were low-pass filtered using a filter with a half-power period of 4 minutes to approximate the 3.5-min averaging of the ADPs. Wave characteristics were not available at the current-profiler sites, so H_{sig} was estimated at each site by interpolating H_{sig} observations in 4 m, 6 m, 8 m and 13 m of water to the water depths of the current profilers. The SandyDuck current profiler sites were generally seaward of the surfzone. Consequently, results are similar if H_{sig} is assumed to not vary between the 13-m and 5-m isobaths and the 8-m array estimate is used for all 7 current profiler sites. Wind observations are from an anemometer at the end of the FRF pier at a height of 19 m. All the SandyDuck time series were averaged to form hourly values.

Wave-driven onshore transport Q_w and hence the predicted depth-averaged offshore flow u_w at all sites were estimated using (3) and the observed significant wave height, dominant wave period, and dominant wave direction. Additionally, the Stokes velocity profile $u_{st}(z,t)$ at the MVCO site was estimated by integrating the observed wave spectrum over the frequency band 0.047–0.5 Hz. The wave transport Q_w, estimated by integrating u_{st} from the surface to the bottom, is well correlated with Q_w estimated from (2) (correlation 0.98), but is 15% smaller. For comparison to the observed average current profiles, the model described in section 2 was forced with the average of the wave forcing vector given by $H_{sig}^2(\cos(\theta_w), \sin(\theta_w))$.

Observed depth-averaged offshore flows below the wave troughs, u_{da}, were estimated from the velocity profiles using a trapezoidal rule and assuming velocities were uniform between the shallowest (deepest) observation and the surface (bottom). Linear extrapolations of the current profiles to the surface and bottom gave similar results (not shown). Wind stress was estimated using the drag coefficient proposed by Smith (1988). To focus on subtidal variability, current time series were detided and then all time series were low-pass filtered using a filter with a 24-hour half-power point (diurnal flows are weak at this site).

The cross-shelf flow is sensitive to the choice of coordinate systems because the flow is strongly polarized along-shelf. The cross-shelf direction at each site is defined here as aligned with the minor principal axis of the depth-averaged subtidal flow (positive offshore), when waves are small ($H_{sig} < 0.75$ m). The resulting offshore direction is roughly perpendicular to the local isobaths and the mean depth-averaged flow during small waves is along-shelf. Only times of small waves were included in estimating the principal axes to determine the coordinate frame orientation because this study shows that surface waves drive a substantial subtidal depth-averaged offshore flow below the wave troughs (section 4a). The subsequent analysis includes all wave conditions.

4. Results

a. Depth-averaged flow

Mean significant wave heights, H_{sig}, are 1.0 m at MVCO and 0.9 m at the SandyDuck sites. Standard deviations of H_{sig} are $\sim$0.5 m at both sites, and wave events typically have time scales of order a day (see u_w in Fig. 4). The largest significant wave heights are 4.5 m during the MVCO deployment and 3.5 m during the Sandy Duck deployment. Average wave periods typically ranged from 4–7 s during the MVCO deployment and 4–16 s during SandyDuck. At MVCO ($h = 12$ m), the maximum $H_{sig}/h = 0.38$ and H_{sig}/h is greater than 0.2 less than 3% of the time, suggesting the MVCO site was always well outside the surfzone. At the 7-m SWWIM site, H_{sig}/h exceeded 0.5 during a few winter storms. There was a notable decrease in H_{sig} between the 12-m and 7-m sites during these events indicating the 7-m site was in

the surfzone. During the SandyDuck study H_{sig}/h was less than 0.5 at all sites, with the exception of one event when the outer edge of the surfzone was at about the 7-m isobath (see section 4b).

Mean depth-averaged cross-shelf flows u_{da} are offshore both south of Martha's Vineyard (0.6–2.0 cm s^{-1}) and off North Carolina (0.6–2.1 cm s^{-1}). Standard deviations of the subtidal cross-shelf flows are 1-2 cm s^{-1} at both sites. Subtidal depth-averaged offshore flows in excess of 2 cm s^{-1} occurred 12% of the time at MVCO, far more often than onshore flows in excess 2 cm s^{-1}, which occurred less than 0.1% of the time (Fig. 4, lower time series).

There is a clear correspondence between the observed depth-averaged offshore flow u_{da} and estimates of the wave-driven offshore flow u_w from (3) (Fig. 4). The correspondence is stronger in shallower water: correlations between subtidal u_{da} and u_w decrease from 0.97 in 5.2-m water depth to $\sim$0 in 27-m water depth (Fig. 5a). Wave forcing accounts for $\sim$50% or more of the variance (correlations greater than 0.7) in u_{da} in water depths of 12 m or less. Linear regression slopes for u_{da} versus u_w are approximately 1.0 with no obvious dependence on water depth (Fig. 5b) and intercepts are less than 1 cm s^{-1} (not shown). The depth-averaged offshore flow decreases with increasing water depth h in a manner consistent with the prediction for undertow from (3) (Fig. 6). Bin averages of the depth-averaged offshore flow as a function of H_{sig}/h exhibit no significant deviation from the wave-driven offshore flow predicted by (3) for the range of water depths and wave heights observed (Fig. 7).

These results are all based on bottom-mounted ADCP current observations. A similar analysis of observations from an earlier inner-shelf study (Lentz et al. 1999) suggests mechanical current meters, such as vector measuring current meters, may not be useful in studying wave-driven flows because of inaccurate averaging of wave orbital velocities (Appendix B).

The agreement between u_{da} and u_w over the inner shelf ($H_{sig}/h < 0.5$) implies that the circulation is two-dimensional (uniform along-shelf) and indicates, as expected, that wave rollers do not make a significant contribution to the onshore volume flux seaward of the surfzone. At the SWWIM 7-m site, u_{da} exceeds u_w during a few events when $H_{sig}/h \approx 0.4$,

supporting the assumption that wave rollers are important in the vicinity of the surfzone, as observed previously (Garcez Faria et al. 2000).

The agreement between u_{da} and u_w also implies a balance between fu and $-fu_{st}$ in the depth-averaged along-shelf momentum balance (10). However, fu and $-fu_{st}$ are not the dominant terms in the subtidal along-shelf momentum balance at MVCO (Fewings 2007). The along-shelf wind stress and along-shelf pressure gradient tend to balance and have subtidal standard deviations that are 2-3 times larger than the other terms, which include temporal acceleration, non-linear advective terms, Coriolis, Hasselmann wave stress, and bottom stress. A detailed examination of the inner shelf momentum balances at MVCO is the subject of a separate manuscript.

The residual subtidal depth-averaged cross-shelf flow, $u_{da} - u_w$, at MVCO has a mean of 0.1 cm s^{-1}, a standard deviation of 0.8 cm s^{-1}, and a maximum magnitude of 4.5 cm s^{-1}. Thus, $u_{da} - u_w$ is generally small relative to the accuracy of the ADCP observations and the uncertainty in the depth-averaged flow estimates. It is striking that there are no large depth-averaged offshore flow events on time scales of days that are inconsistent with undertow in either the Martha's Vineyard or North Carolina observations. In summary, the observed, subtidal, depth-averaged offshore flows in water depths less than about 20 m are consistent with wave-driven undertow given by (3).

b. Vertical structure

The vertical structure of the offshore flow varies across the inner shelf for the SandyDuck event shown in Fig. 8. Based on the observed onshore decrease in H_{sig}, or on $H_{sig}/h \approx 0.5$, the offshore edge of the surfzone during this event is between the 6-m and 8-m isobaths. At the two shallow sites within the surfzone (water depths 5.2 m and 6.5 m), the maximum offshore flow is near the bottom. Between 600 m and 1200 m offshore, the offshore flow is vertically uniform, while at the site farthest offshore, the maximum offshore flow is in the upper half of the water column. This cross-shelf variation in the vertical structure is qualitatively consistent with previous theory, laboratory results, and ocean observations (Nadaoka and

Kondoh 1982; Putrevu and Svendsen 1993; Reniers et al. 2004). However, an onshore and southward wind stress $\boldsymbol{\tau}^s$ during this event ($\tau^{sx} \approx -0.09$ N m^{-2} and $\tau^{sy} \approx -0.44$ N m^{-2}) undoubtedly influenced the vertical structure of the offshore flow (see also Newberger and Allen 2007b).

The long time series at MVCO allows us to separate wind- and wave-driven cross-shelf flows. The wind stress has a substantial impact on the vertical structure of the cross-shelf flow at MVCO (Fewings et al. 2008). During moderate waves (1 m $< H_{sig} < 2$ m) and weak wind stresses (defined as $|\boldsymbol{\tau}^s| < 0.03$ N m^{-2}), the mean cross-shelf flow profile has maximum flow and larger vertical shear near the surface, and smaller shear and weak flow near the bottom (Fig. 9). During onshore wind stresses, the average cross-shelf flow profile is less sheared because the wind-driven shear opposes the wave-driven shear. During offshore wind stresses, the average cross-shelf profile is more sheared because the wind-driven shear enhances the wave-driven shear. Fewings et al. (2008) examine the response of the cross-shelf circulation to wind stress and to combined wind stress and wave forcing using the MVCO observations. Since the focus here is on wave-driven cross-shelf flows, the remainder of the analyses focus on the MVCO current profiles during times when the wind stress is weak ($|\boldsymbol{\tau}^s| < 0.03$ N m^{-2}).

When the wind stress is weak and the waves are small ($H_{sig} < 0.75$ m), the depth-averaged flow is approximately zero (section 4a) but there is still a vertically sheared cross-shelf flow with offshore flow in the upper half of the water column and onshore flow in the lower half of the water column (Fig. 10a). The cross-shelf flow profiles for summer (April–September) and winter (October–March) are similar, with slightly more shear in the summer profile. The corresponding mean along-shelf flow is westward and vertically sheared with maximum flow near the surface (Fig. 10b). The summer and winter profiles have similar near-bottom along-shelf velocities, but the summer profile is strongly sheared with a near-surface along-shelf velocity of 8 cm s^{-1} while the winter profile is nearly vertically uniform. The vertical shear in the along-shelf flow is probably in thermal wind balance with the cross-shelf density gradient, which varies seasonally (Lentz et al. 1999; Shearman and Lentz 2003). The mean

current profiles during weak winds and small waves are similar to mean current profiles throughout the Middle Atlantic Bight (Lentz 2007). The cause of the mean flow structure during weak wind and wave forcing is not known, but it may be related to an along-shelf pressure gradient (Lentz 2007). To focus on wave-driven flows, the mean flow profiles during weak winds and small waves are subtracted from the observed profiles in the remainder of the analysis here and in section 5.

Bin-averaged cross-shelf velocity profiles for different ranges of H_{sig} ($|\boldsymbol{\tau}^s| < 0.03$ N m^{-2}) exhibit a similar vertical structure with maximum offshore velocity near the surface (Fig. 11a). The strength of the offshore flow increases with increasing H_{sig}, as noted in section 4a. The observed offshore flow profiles are more consistent with the model profiles for small eddy viscosities (Fig. 3 $A < 10^{-3}$ m^2 s^{-1}, see also Appendix A Fig. 14) than with the parabolic model profiles for large eddy viscosities (Fig. 3 $A \geq 10^{-3}$ m^2 s^{-1}) observed in the surfzone. In fact, the model profiles with small eddy-visosity ($A = 10^{-5}$ m^2 s^{-1}), or the $-u_{st}$ profiles determined from the average significant wave height, wave period, and wave direction, accurately reproduce the magnitude and vertical structure of the bin-averaged cross-shelf velocity profiles (Fig. 11a).

The observed along-shelf velocity profiles exhibit a less consistent pattern (Fig. 11b). For H_{sig} between 0.75 m and 2.25 m the average along-shelf velocities are small (generally 1 cm s^{-1} or less), while for H_{sig} between 2.25 m and 3 m there is a mean westward flow of about 4 cm s^{-1} with a maximum at mid-depth. The model profiles roughly agree in magnitude and shape with the observed bin-averaged profiles except for the bin with H_{sig} between 1.5 m and 2.25 m. This discrepancy may be related to seasonal variations in the flow.

There is a notable difference between observed average summer and winter current profiles during weak winds (Fig. 12). Average summer profiles of both u and v are more sheared than winter profiles. Average cross-shelf flows for winter and summer are similar near the surface but the near-bottom flow is weakly onshore in summer and offshore in winter. The average along-shelf flow is vertically uniform in winter but reverses in summer from 1 cm s^{-1} westward

near the bottom to 1 cm s^{-1} eastward near the surface (relative to the corresponding weak forcing profiles in Fig. 10). The model profiles reproduce the observed structure of the winter profiles, though overestimating the along-shelf velocity, but do not reproduce the observed summer velocity profiles. As discussed below, the dynamics associated with the summer current profiles are unclear.

5. Discussion

a. Seasonal variations in observed profiles

The agreement between the observed winter profile and the model profiles with relatively small eddy viscosities is somewhat surprising given that vertical mixing may be large at this site in winter. Semidiurnal tidal currents are strong (25 cm s^{-1}) in the along-shelf direction, which suggests tidal mixing may be substantial. However, the vertical shear in the cross-shelf flow is larger during spring tides (relatively large tidal currents) than during neap tides (Fewings et al. 2008). There are also strong surface cooling events in winter that should drive convection. The vertical shear in the average cross-shelf flow does decrease for increased surface cooling, as expected.

The average summer cross-shelf velocity profile is more vertically sheared than either the winter or the model profiles (Fig. 12a). Since the relevant model response is essentially inviscid ($A \approx 0$), suppression of turbulent mixing by the stratification does not seem to explain the discrepancy; the observed profiles have more shear than the inviscid model response. However, the over-simplified model does not consider spatial variations in the wave forcing or response, buoyancy forcing, or other potentially important elements of the dynamics such as the relative vorticity of the mean flow (*e.g.* McWilliams et al. 2004). For example, vertical mixing and the cross-shelf circulation acting on the stratification may influence the dynamics by creating buoyancy forcing similar to the stratified inner-shelf response to wind forcing (Austin and Lentz 2002). The influence of stratification and vertical mixing processes in both winter and summer is a focus of the ongoing SWWIM project that includes obtaining moored observations of the stratification throughout the year and

numerical modeling.

b. Cross-shelf exchange

It is worth considering how the wave-driven Eulerian cross-shelf transport (Q_w) compares to wind-driven cross-shelf transport. Previous studies have shown that at mid shelf the cross-shelf transport in the surface boundary layer driven by an along-shelf wind stress (Q_τ) is roughly equal to the Ekman transport $U_E = \tau^{sy}/\rho_\circ f$ (*e.g.*, Smith 1981; Lentz 1992; Shearman and Lentz 2003). To estimate the relative importance of wave and wind-driven cross-shelf transport, consider

$$\frac{Q_w}{U_E} = \frac{\rho_\circ g f}{16c} \frac{H_{sig}^2}{\tau^{sy}} \tag{14}$$

with $\theta_w = 180°$. For both SandyDuck and MVCO, H_{sig}^2 and τ^{sy} are significantly correlated at the 95% confidence level with regression slopes of 20–30 m^4 N^{-1}. Assuming $H_{sig}^2/\tau^{sy} = 25$ m^4 N^{-1}, Q_w is 10–20% of U_E, depending on the wave period, for water depths greater than about 10 m (Fig. 13). Two recent studies found that the observed cross-shelf transport above the first zero crossing in the cross-shelf flow decreases from roughly U_E at the 30–50-m isobath toward zero in shallow water (Lentz et al. 2001; Kirincich et al. 2005) consistent with the expected decrease in the wind-driven transport in shallow water (Ekman 1905). The observed transports were assumed to be due to the along-shelf wind stress but neither surface gravity wave forcing nor cross-shelf wind stresses were considered, both of which are correlated with the along-shelf wind stress (Fewings et al. 2008). The decrease in Q_τ as the depth decreases combined with the increase in Q_w as the depth decreases suggests that shallower than some critical water depth Q_w will exceed Q_τ. For a simple model case (Fig. 13; $\tau^{sy} = 0.1$ N m^{-2}, $H_{sig}^2/\tau^{sy} = 25$ m^4 N^{-1}, and an unstratified turbulent eddy-viscosity profile), Q_w is greater than Q_τ for water depths less than 20 m. In general, this critical depth will depend on the width of the inner shelf (*i.e.*, the region over which the wind-driven transport is reduced) and hence on the strength of the wind and wave forcing and the stratification (Lentz 1995; Austin and Lentz 2002).

Though the observed Eulerian wave-driven cross-shelf transport can be substantial over

the inner shelf, it may not be effective at driving cross-shelf exchange. Net Lagrangian particle transports are due to the sum of the Eulerian flow and the Stokes drift. Since the mean Eulerian and Stokes drift profiles are nearly equal in winter, but have opposite directions ($u \approx -u_{st}$), the net cross-shelf exchange due to waves is probably small. The larger discrepancy between u and u_{st} in the summer mean profiles (Fig. 12a) suggests a larger cross-shelf exchange. The combined influence of wind and wave forcing on Lagrangian transport is discussed by Fewings et al. (2008).

6. Summary

Observations from two sites along the East Coast of the United States provide compelling evidence that the depth-averaged offshore flow (below the wave troughs) seaward of the surfzone, in water depths of 5–13 m, is primarily undertow driven by surface gravity waves, not by wind forcing. The evidence for this is the significant correlations between the predicted (from equation 3) and observed depth-averaged cross-shelf flows (Fig. 5) and the consistency with theory of the dependence of the observed depth-averaged offshore flow on both water depth and wave height (Figs. 6 and 7).

The observed average cross-shelf velocity profile seaward of the surfzone forced by waves (during weak wind stresses) has maximum offshore flow and vertical shear near the surface, and weak offshore flow and vertical shear in the lower half of the water column (Fig. 11a). This vertical structure of the cross-shelf flow seaward of the surfzone does not resemble the parabolic profiles with maximum offshore flow at mid-depth or near the bottom observed in the surfzone (Fig. 1a; Haines and Sallenger 1994; Garcez Faria et al. 2000; Reniers et al. 2004). Instead, the observed cross-shelf velocity profiles seaward of the surfzone during winter are consistent with an inviscid balance between the Coriolis force associated with the offshore flow and the Hasselmann wave stress associated with the influence of the Earth's rotation on surface waves (Figs. 1b and 11a). The agreement provides some of the first direct observational evidence for the importance of the Hasselmann wave stress in forcing oceanic flows. Average summer cross-shelf velocity profiles are more sheared than either average

winter profiles or model profiles (Fig. 12). Suppression of turbulent stresses by the stronger summer stratification does not appear to be the explanation, since the assumed momentum balance is essentially inviscid. Observations and model studies of undertow during stratified conditions over the inner shelf are needed to understand the dynamics of the summer profiles.

Given the fundamental nature of the wave-driven transport, it seems likely that undertow will be present on most inner shelves exposed to waves. Wave-driven undertow is likely to be significant relative to wind-driven cross-shelf flows in water depths less than about 20 m (Fig. 5 and 13). The observed cross-shelf velocities of a few centimeters per second associated with wave forcing over the inner shelf suggest flushing times of a day or less. However, since the Stokes drift associated with the surface gravity waves opposes the observed Eulerian flow, the wave-driven flow may be a less effective mechanism for particle exchange than suggested by the observed Eulerian flows. The connection between undertow within and offshore of the surfzone and the resulting particle transport between the surfzone and the inner shelf is an important unresolved problem.

Appendix A: Numerical model

Equations (1), (9), and (10) were also solved numerically using a control volume approach on a logarithmic vertical grid with 1001 grid points. The numerical model was run for unstratified flows with "realistic" eddy-viscosity profiles, in which the shape of the eddy-viscosity profile is prescribed, but the magnitude of the eddy viscosity depends on the surface and bottom stresses (details regarding the numerical scheme and eddy-viscosity profiles are given in Lentz 1995). The eddy viscosity profiles are assumed to only depend on the "mean" flow stress at the surface and bottom since the wave-driven mixing is confined to very thin wave boundary layers (Trowbridge and Agrawal 1995). A bottom roughness of $z_o = 10^{-3}$ m was used.

As a test, the numerical model was also run using constant eddy viscosities. Velocity profiles from the numerical model with constant eddy viscosities are essentially identical to the analytic solutions.

For $H_{sig} = 1 - 4$ m, a wave period of 7 sec and a water depth of 12 m, the cross-shelf velocity profiles from the numerical model are similar for the different forms of the eddy-viscosity profiles and resemble the cross-shelf velocity profiles for small constant eddy viscosities ($A \leq 10^{-4}$ m^2 s^{-1} in Fig. 3), except near the boundaries (Fig. 14b). This result is not surprising since $u \approx -u_{st}$ is independent of the eddy viscosity, provided the eddy viscosity (or δ_E/h) is small. The along-shelf velocities are more sensitive to the form of the eddy viscosity (Fig. 14c).

Appendix B: Mechanical current meter response and wave-bias errors

The 1994 Coastal Ocean Processes Inner Shelf Study (CoOP94) on the North Carolina shelf (Lentz et al. 1999), at the same location as the 1997 SandyDuck study, offers another opportunity to examine wave-driven cross-shelf flows. However, analysis of the observations suggests wave-bias errors in mechanical current meters are too large to make them useful for studying wave-driven flows. The CoOP94 study included five sites instrumented with

current meters, as well as wave measurements from the Army Corps of Engineers Field Research Facility. Towers of electromagnetic current meters (EMCM) were deployed in 4-m and 8-m water depth, and moorings supporting vector-measuring current meters (VMCM) were deployed in 13-m, 21-m, and 26-m water depth. The EMCMs measure currents by sensing changes in the electromagnetic field induced by the ocean water flowing past the instrument. The VMCMs are mechanical current meters consisting of two propellers oriented perpendicular to each other, and were specifically designed to accurately average oscillating flows associated with surface waves (Weller and Davis 1980). Nevertheless, the VMCMs are known to have wave-bias errors of a few cm s^{-1} caused by the passage of the propellers through their own wake in an oscillating flow (Weller and Davis 1980; Beardsley 1987).

Comparison of the measured depth-averaged currents with the predicted wave-driven undertow for the 4-m and 8-m sites, where EMCMs were deployed, are similar to results from the ADCPs deployed during the SandyDuck study (Fig. 15). Correlations between the observed and predicted offshore flow are 0.6–0.8 and regression coefficients are near 1. The lower correlations for the EMCMs is presumably because there is much poorer vertical coverage (only 4 depths at the 4-m site and 7 depths at the 8-m site, with only 3 current meters working for most of the deployment). The correlations for the VMCM instrumented sites are negative (-0.3 to -0.6), rather than positive, and regression coefficients range from -1 to -5. Note the difference between the ADCP and VMCM correlations and regression coefficients in 12 - 13 m water depth. The discrepancy between the ADCP and VMCM results from the North Carolina inner shelf is in sharp contrast to the consistent ADCP results from the North Carolina and Martha's Vineyard inner shelves in Fig. 5. It seems likely that the VMCM results are due to wave bias errors. Given that VMCMs average oscillating flows more accurately than most mechanical current meters (Weller and Davis 1980), it seems unlikely that previous studies using mechanical current meters will be useful in studying wave-driven flows over the inner shelf.

References

Ardhuin, F., B. Chapron, and T. Elfouhaily, 2004: Waves and the air-sea momentum budget: Implications for ocean circulation modeling. *J. Phys. Oceanogr.*, **34**, 1741–1755.

Austin, J. A., and S. J. Lentz, 2002: The inner shelf response to wind-driven upwelling and downwelling. *J. Phys. Oceanogr.*, **32**, 2171–2193.

Beardsley, R. C., 1987: A comparison of the vector-averaging current meter and new Edgerton, Germeshausen, and Grier, Inc., vector-measuring current meter on a surface mooring in CODE 1. *J. Geophys. Res.*, **92**, 1845–1860.

Ekman, V. W., 1905: On the influence of the earth's rotation on ocean currents. *Ark. Mat. Aston. Fys.*, **2**, 1–53.

Fewings, M., 2007: Cross-shelf circulation and momentum and heat balances over the inner continental shelf near Martha's Vineyard, Massachusetts. Ph.D. thesis, MIT/WHOI Joint Program, Woods Hole, Massachusetts. 267 pp.

Fewings, M., S. J. Lentz, and J. Fredericks, 2008: Observations of cross-shelf flow driven by cross-shelf winds on the inner continental shelf. *J. Phys. Oceanogr.*, **submitted**.

Garcez Faria, A. F., E. B. Thornton, T. C. Lippman, and T. P. Stanton, 2000: Undertow over a barred beach. *J. Geophys. Res.*, **105**, 16 999–17 010.

Govender, K., G. P. Mocke, and M. J. Alport, 2002: Video-imaged surf zone wave and roller structures and flow fields. *J. Geophys. Res.*, **107**, 3072,doi10.1029/2000JC000 755.

Haines, J. W., and A. H. Sallenger, Jr., 1994: Vertical structure of mean cross-shore currents across a barred surf zone. *J. Geophys. Res.*, **99**, 14 223–14 242.

Hasselmann, K., 1970: Wave-driven inertial oscillations. *Geophy. Fluid Dyn.*, **1**, 463–502.

Kirincich, A. R., J. A. Barth, B. A. Grantham, B. A. Menge, and J. Lubchenco, 2005: Wind-driven inner-shelf circulation off central Oregon during summer. *J. Geophys. Res.*, **110**, doi:10.1029/2004JC002 611.

LeBlond, P. H., and L. A. Mysak, 1978: *Waves in the ocean*. Elsevier Scientific Publishing Company.

Lee, T. N., E. Williams, R. E. J. Wang, and L. Atkinson, 1989: Response of South Carolina continental shelf waters to wind and Gulf Stream forcing during winter of 1986. *J. Geophys. Res.*, **94**, 10 715–10 754.

Lentz, S. J., 1992: The surface boundary layer in coastal upwelling regions. *J. Phys. Oceanogr.*, **22**, 1517–1539.

Lentz, S. J., 1994: Current dynamics over the northern California inner shelf. *J. Phys. Oceanogr.*, **24**, 2461–2478.

Lentz, S. J., 1995: Sensitivity of the inner-shelf circulation to the eddy-viscosity profile. *J. Phys. Oceanogr.*, **25**, 19–28.

Lentz, S. J., 2007: Observations of the mean circulation over the Middle Atlantic Bight continental shelf. *J. Phys. Oceanogr.*, **accepted**.

Lentz, S. J., M. Carr, and T. H. C. Herbers, 2001: Barotropic tides on the North Carolina shelf. *J. Phys. Oceanogr.*, **31**, 1843–1859.

Lentz, S. J., R. T. Guza, S. Elgar, F. Feddersen, and T. H. C. Herbers, 1999: Momentum balances on the North Carolina inner shelf. *J. Geophys. Res.*, **104**, 18 205–18 226.

Lentz, S. J., K. Shearman, S. Anderson, A. Plueddemann, and J. Edson, 2003: The evolution of stratification over the New England shelf during the Coastal Mixing and Optics study, August 1996 - June 1997. *J. Geophys. Res.*, **108**, doi:10.1029/2001JC001 121.

Lentz, S. J., and C. D. Winant, 1986: Subinertial currents on the southern California shelf. *J. Phys. Oceanogr.*, **16**, 1737–1750.

Longuet-Higgins, M. S., 1953: Mass transport in water waves. *Phil. Trans. Roy. Soc. London A*, **245**, 535–581.

Longuet-Higgins, M. S., and R. W. Stewart, 1964: Radiation stresses in water waves; a physical discussion, with applications. *Deep Sea Res.*, **11**, 529–562.

Masselink, G., and K. P. Black, 1995: Magnitude and cross-shore distribution of bed return flow measured on natural beaches. *Coastal Eng.*, **25**, 165–190.

McWilliams, J. C., and J. M. Restrepo, 1999: The wave-driven ocean circulation. *J. Phys. Oceanogr.*, **29**, 2523–2540.

McWilliams, J. C., J. M. Restrepo, and E. M. Lane, 2004: An asymptotic theory for the interaction of waves and currents in coastal waters. *J. Fluid Mech.*, **511**, 135–178.

Mei, C. C., 1983: *The applied dynamics of ocean surface waves*. John Wiley & Sons, Inc.

Nadaoka, K., and T. Kondoh, 1982: Laboratory measurements of velocity field structures in the surfzone by LDV. *Coastal Eng. Jpn*, **25**, 125–145.

Newberger, P. A., and J. S. Allen, 2007a: Forcing a three-dimensional, hydrostatic primitive-equation model for application in the surf zone, Part 1: Formulation. *J. Geophys. Res.*, **112**, C08 018, doi:10.1029/2006JC003 472.

Newberger, P. A., and J. S. Allen, 2007b: Forcing a three-dimensional, hydrostatic primitive-equation model for application in the surf zone, Part 2: Application to DUCK94. *J. Geophys. Res.*, **112**, C08 019, doi:10.1029/2006JC003 474.

Polton, J. A., D. M. Lewis, and S. E. Belcher, 2005: The role of wave-induced Coriolis-Stokes forcing on the wind-driven mixed layer. *J. Phys. Oceanogr.*, **35**, 444–457.

Putrevu, U., and I. A. Svendsen, 1993: Vertical structure of the undertow outside the surf zone. *J. Geophys. Res.*, **98**, 22 707–22 716.

Reniers, A. J. H. M., E. B. Thornton, T. P. Stanton, and J. A. Roelvink, 2004: Vertical flow structure during Sandy Duck: observations and modeling. *Coastal Eng.*, **51**, 237–260.

Shearman, R. K., and S. J. Lentz, 2003: Dynamics of mean and subtidal flow on the New England shelf. *J. Geophys. Res.*, **108**, 3281, doi:10.1029/2002JC001 417.

Smith, J. A., 2006: Wave-current interactions in finite depth. *J. Phys. Oceanogr.*, **36**, 1403–1419.

Smith, R. L., 1981: A comparison of the structure and variability of the flow field in three coastal upwelling regions: Oregon, Northwest Africa, and Peru. F. A. Richards, Ed., *Coastal Upwelling*, American Geophysical Union, 107–118.

Smith, R. L., 1988: Coefficients for sea surface wind stress, heat flux, and wind profiles as a function of wind speed and temperature. *J. Geophys. Res.*, **93**, 15 467–15 472.

Stive, M., and H. Wind, 1986: Cross-shore mean flow in the surfzone. *Coastal Eng.*, **10**, 325–340.

Stokes, G. G., 1847: On the theory of oscillatory waves. *Trans. Camb. Phil. Soc.*, **8**, 441–455.

Svendsen, I. A., 1984: Mass flux and undertow in a surf zone. *Coastal Engineering*, **8**, 347–365.

Ting, F. C. K., and J. T. Kirby, 1994: Observations of undertow and turbulence in a laboratory surf zone. *Coastal Eng.*, **24**, 51–80.

Trowbridge, J. H., and Y. C. Agrawal, 1995: Glimpses of a wave boundary layer *J. Geophys. Res.*, **100**, 20729–20743.

Weller, R. A., and R. E. Davis, 1980: A vector-measuring current meter. *Deep Sea Res.*, **27**, 575–582.

Winant, C. D., 2006: Three-dimensional wind-driven coastal circulation past a headland. *J. Phys. Oceanogr.*, **36**, 1430–1438.

Wright, L. D., R. T. Guza, and A. D. Short, 1982: Dynamics of a high-energy dissipative surf zone. *Mar. Geology*, **45**, 41–62.

Xu, Z., and A. J. Bowen, 1994: Wave- and wind-driven flow in water of finite depth. *J. Phys. Oceanogr.*, **24**, 1850–1866.

Figure 1 Schematics of (a) a parabolic offshore flow profile consistent with (12) and (b) an offshore flow profile ($u = -u_{st}$) driven by the Hasselmann wave stress given by (7). The parabolic profile (a) is often observed in the surfzone and is associated with relatively strong vertical mixing when the Earth's rotation is not dynamically important. The Hasselmann profile (b) is associated with relatively weak vertical mixing and the Earth's rotation is dynamically important through both the Coriolis force and the wave forcing.

Figure 2 Contributions to the average (a) cross-shelf u and (b) along-shelf v velocity profiles from the surface wave stress τ^{ws}, the near-bottom wave stress τ^{wb}, the Hasselmann wave stress τ^{wH}, and sum of the cross-shelf pressure gradient and momentum flux divergence due to wave shoaling $-g\eta_x + F^{ws}$. Model profiles were computed for a significant wave height of 2 m, wave period of 7 s, water depth of 12 m and an eddy viscosity of 10^{-5} m^2 s^{-1}.

Figure 3 Average (a) cross-shelf and (b) along-shelf velocity profiles from the model described in section 2 for a range of constant eddy viscosities A from 10^{-6} m^2 s^{-1} to 1 m^2 s^{-1}. These values of A correspond to δ_E/h ranging from approximately 0.01 to 10, where δ_E is the Ekman boundary layer scale and h is the water depth. Model profiles were computed for a significant wave height of 2 m, wave period of 7 s, and water depth of 12 m.

Figure 4 Observed depth-averaged cross-shelf flow u_{da} over a four month period from the Martha's Vineyard Coastal Observatory (water depth 12 m) and the depth-averaged wave-driven offshore flow u_w (dashed line) estimated using (3) and the observed wave characteristics. Time series of u_w has been offset $+6$ cm s^{-1} for clarity.

Figure 5 The (a) correlation and (b) regression slope a from linear regressions of the form $u_{da} = au_w + b$ for the seven SandyDuck sites and the MVCO and SWWIM sites. All correlations in (a) are significant at the 95% confidence level with the exception of the 27-m site. The error bars in (b) correspond to the 95% confidence intervals on the regression slope estimates. Intercepts are all less than 1 cm s^{-1}.

Figure 6 Linear regression slope of u_{da} versus H_{sig}^2 as a function of water depth for the seven

SandyDuck sites and MVCO. Dashed line is theoretical dependence of u_w/H_{sig}^2 on water depth based on (3) assuming shallow water waves ($c = \sqrt{gh}$). The error bars indicate the 95% confidence intervals on the regression slope estimates.

Figure 7 Bin averages of normalized depth-averaged offshore flow as a function of H_{sig}/h for the MVCO current observations and individual daily averages for all the SandyDuck sites. The dashed line is the theoretical prediction from (3). The current observations are from sites seaward of the offshore edge of the surfzone, which is roughly at $H_{sig}/h \approx 0.5$. The error bars indicate the standard errors of the bin averages for the MVCO observations.

Figure 8 Offshore section showing the bathymetry, locations of the ADCPs deployed during SandyDuck (triangles), and an example of the wave-driven offshore flow averaged over the time period 17:00 – 23:00 19 October 1997, when the average significant wave height was 3.3 m. The offshore edge of the surfzone is at about the 7-m isobath. A schematic of the corresponding linear, monochromatic wave (10-s period) is also shown assuming no dissipation outside the surfzone and saturated wave heights within the surfzone such that $H_{sig} = h/2$. Bathymetry within 1000 m of the coast is from a survey taken August 13, 1997 and farther offshore from a ship survey conducted in the fall of 1994.

Figure 9 Average offshore flow profiles from MVCO for periods when 1 m $< H_{sig} <$ 2 m, and the wind stress was either offshore (0.1 N m^{-2} $< \tau^{sx} <$ 0.2 N m^{-2}), onshore (-0.2 N m^{-2} $< \tau^{sx} <$ -0.1 N m^{-2}), or weak ($|\tau^s| <$ 0.03 N m^{-2}).

Figure 10 Average (a) cross-shelf u and (b) along-shelf v velocity profiles from MVCO for periods when the waves are small ($H_{sig} <$ 0.75 m) and the wind stress is weak ($|\tau^s| <$ 0.03 N m^{-2}), for all data, summer (April–September), and winter (October–March).

Figure 11 Average (a) cross-shelf u and (b) along-shelf v velocity profiles from MVCO for different ranges of H_{sig} during periods when the wind stress magnitude was small ($|\tau^s| <$ 0.03 N m^{-2}) and corresponding model profiles (dashed lines) estimated using the average wave characteristics for each range of H_{sig} and a constant eddy viscosity of $A = 10^{-5}$ m^2 s^{-1}.

Observed profiles for $H_{sig} < 0.75$ m are zero because the weak wind and small wave mean profile (Fig. 10) has been subtracted from all profiles. Standard errors of the means for the observed profiles are 0.1 cm s^{-1} for $0 < H_{sig} < 0.75$ and $0.75 < H_{sig} < 1.5$, 0.4 cm s^{-1} for $1.5 < H_{sig} < 2.25$, and 1.6 cm s^{-1} for $2.25 < H_{sig} < 3.5$. The reduced offshore currents in the top bin (height 10 m) may be due to contamination by surface reflections from the side-lobes of the ADCP acoustic pulses during large waves because of the reduced water depth under the wave troughs.

Figure 12 Average (a) cross-shelf u and (b) along-shelf v velocity profiles from MVCO for 1 m$< H_{sig} < 2$ m and $|\boldsymbol{\tau}^s| < 0.03$ N m^{-2} during winter (October–March) and summer (April–September) and from the model for $A = 10^{-5}$ m^2 s^{-1} using the average wave characteristics for the selected observations. Only the average model profile is shown because the summer and winter model profiles are similar since the average wave characteristics are essentially the same. Standard errors of the means are 0.3 cm s^{-1} for the winter profile and 0.5 cm s^{-1} for the summer profile.

Figure 13 The wave-driven transport (Q_w) normalized by the Ekman transport (U_E) as a function of water depth for wave periods of 5, 10, and 15 s estimated from (14) assuming $H_{sig}^2/\tau^{sy} = 25$ m^4 N^{-1} (dashed lines). The solid line shows the normalized cross-shelf transport (Q_τ) driven by an along-shelf wind stress $(\tau^{sy} = 0.1$ N m$^{-2})$ as a function of water depth from a two-dimensional model (no along-shelf variation) with an unstratified turbulent eddy viscosity that increases linearly from zero at each boundary over 10% of the boundary layer thickness and is constant in the interior (see Lentz 1995).

Figure 14 Profiles of (a) eddy viscosity A, (b) cross-shelf velocity u and (c) along-shelf velocity v from the numerical model for $H_{sig} = 2$ m, wave period of 7 s, water depth of 12 m, and bottom roughness of $z_o = 10^{-3}$ m.

Figure 15 The (a) correlation and (b) regression slope a from linear regressions of the form $u_{da} = a u_w + b$ for electromagnetic current meters (EMCM) and vector-measuring current meters (VMCM) deployed in 1994 on the North Carolina shelf and acoustic Doppler current

profilers (ADCP) deployed at the same site in 1997. The error bars in (b) correspond to the 95% confidence intervals on the regression slope estimates. The negative correlations and regression slopes for the VMCMs are probably due to bias errors caused by inaccurate mechanical averaging of wave velocities.
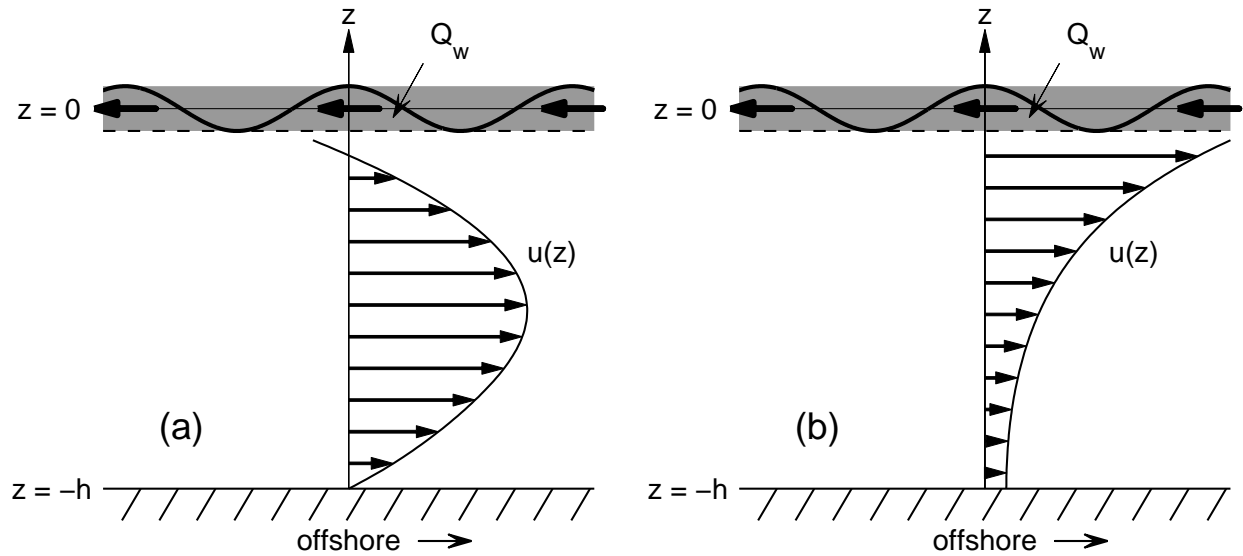
Figure 1: Schematics of (a) a parabolic offshore flow profile consistent with (12) and (b) an offshore flow profile ($u = -u_{st}$) driven by the Hasselmann wave stress given by (7). The parabolic profile (a) is often observed in the surfzone and is associated with relatively strong vertical mixing when the Earth's rotation is not dynamically important. The Hasselmann profile (b) is associated with relatively weak vertical mixing and the Earth's rotation is dynamically important through both the Coriolis force and the wave forcing.

Figure 2: Contributions to the average (a) cross-shelf u and (b) along-shelf v velocity profiles from the surface wave stress τ^{ws}, the near-bottom wave stress τ^{wb}, the Hasselmann wave stress τ^{wH}, and sum of the cross-shelf pressure gradient and momentum flux divergence due to wave shoaling $-g\eta_x + F^{ws}$. Model profiles were computed for a significant wave height of 2 m, wave period of 7 s, water depth of 12 m and an eddy viscosity of 10^{-5} m^2 s^{-1}.

Figure 3: Average (a) cross-shelf and (b) along-shelf velocity profiles from the model described in section 2 for a range of constant eddy viscosities A from 10^{-6} m^2 s^{-1} to 1 m^2 s^{-1}. These values of A correspond to δ_E/h ranging from approximately 0.01 to 10, where δ_E is the Ekman boundary layer scale and h is the water depth. Model profiles were computed for a significant wave height of 2 m, wave period of 7 s, and water depth of 12 m.

Figure 4: Observed depth-averaged cross-shelf flow u_{da} over a four month period from the Martha's Vineyard Coastal Observatory (water depth 12 m) and the depth-averaged wave-driven offshore flow u_w (dashed line) estimated using (3) and the observed wave characteristics. Time series of u_w has been offset $+6$ cm s^{-1} for clarity.

Figure 5: The (a) correlation and (b) regression slope a from linear regressions of the form $u_{da} = au_w + b$ for the seven SandyDuck sites and the MVCO and SWWIM sites. All correlations in (a) are significant at the 95% confidence level with the exception of the 27-m site. The error bars in (b) correspond to the 95% confidence intervals on the regression slope estimates. Intercepts are all less than 1 cm s^{-1}.

Figure 6: Linear regression slope of u_{da} versus H_{sig}^2 as a function of water depth for the seven SandyDuck sites and MVCO. Dashed line is theoretical dependence of u_w/H_{sig}^2 on water depth based on (3) assuming shallow water waves ($c = \sqrt{gh}$). The error bars indicate the 95% confidence intervals on the regression slope estimates.

Figure 7: Bin averages of normalized depth-averaged offshore flow as a function of H_{sig}/h for the MVCO current observations and individual daily averages for all the SandyDuck sites. The dashed line is the theoretical prediction from (3). The current observations are from sites seaward of the offshore edge of the surfzone, which is roughly at $H_{sig}/h \approx 0.5$. The error bars indicate the standard errors of the bin averages for the MVCO observations.
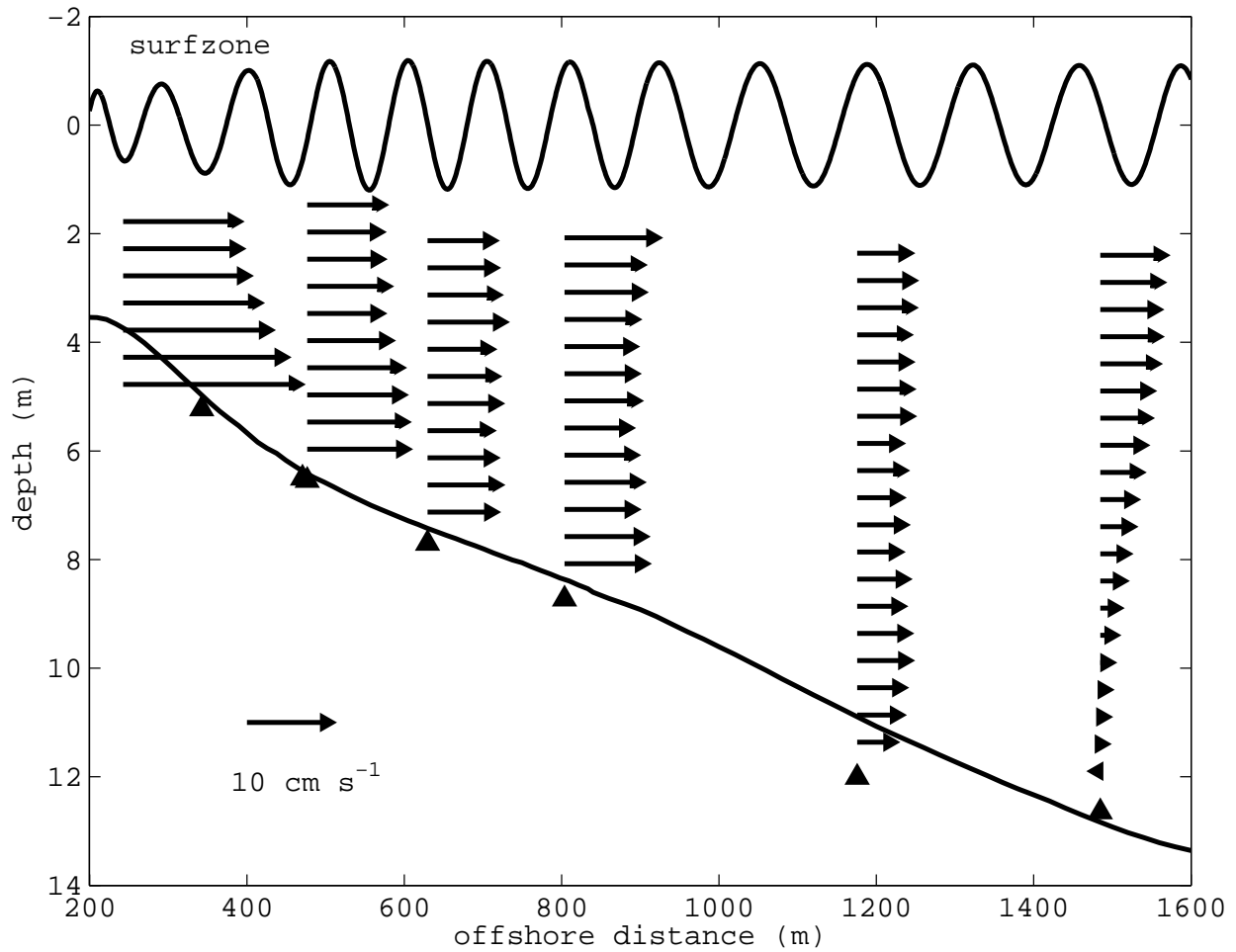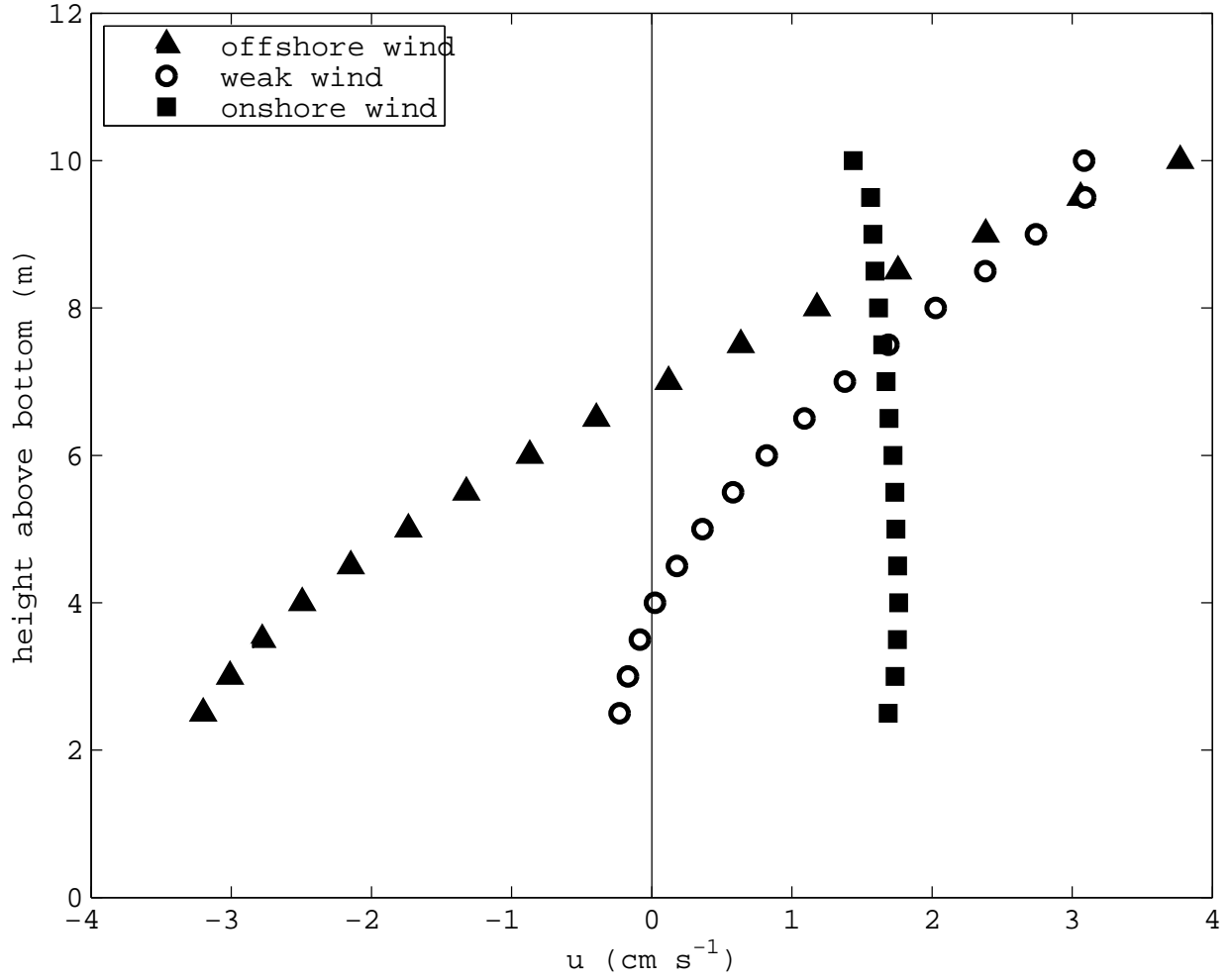
Figure 8: Offshore section showing the bathymetry, locations of the ADCPs deployed during SandyDuck (triangles), and an example of the wave-driven offshore flow averaged over the time period 17:00 – 23:00 19 October 1997, when the average significant wave height was 3.3 m. The offshore edge of the surfzone is at about the 7-m isobath. A schematic of the corresponding linear, monochromatic wave (10-s period) is also shown assuming no dissipation outside the surfzone and saturated wave heights within the surfzone such that $H_{sig} = h/2$. Bathymetry within 1000 m of the coast is from a survey taken August 13, 1997 and farther offshore from a ship survey conducted in the fall of 1994.
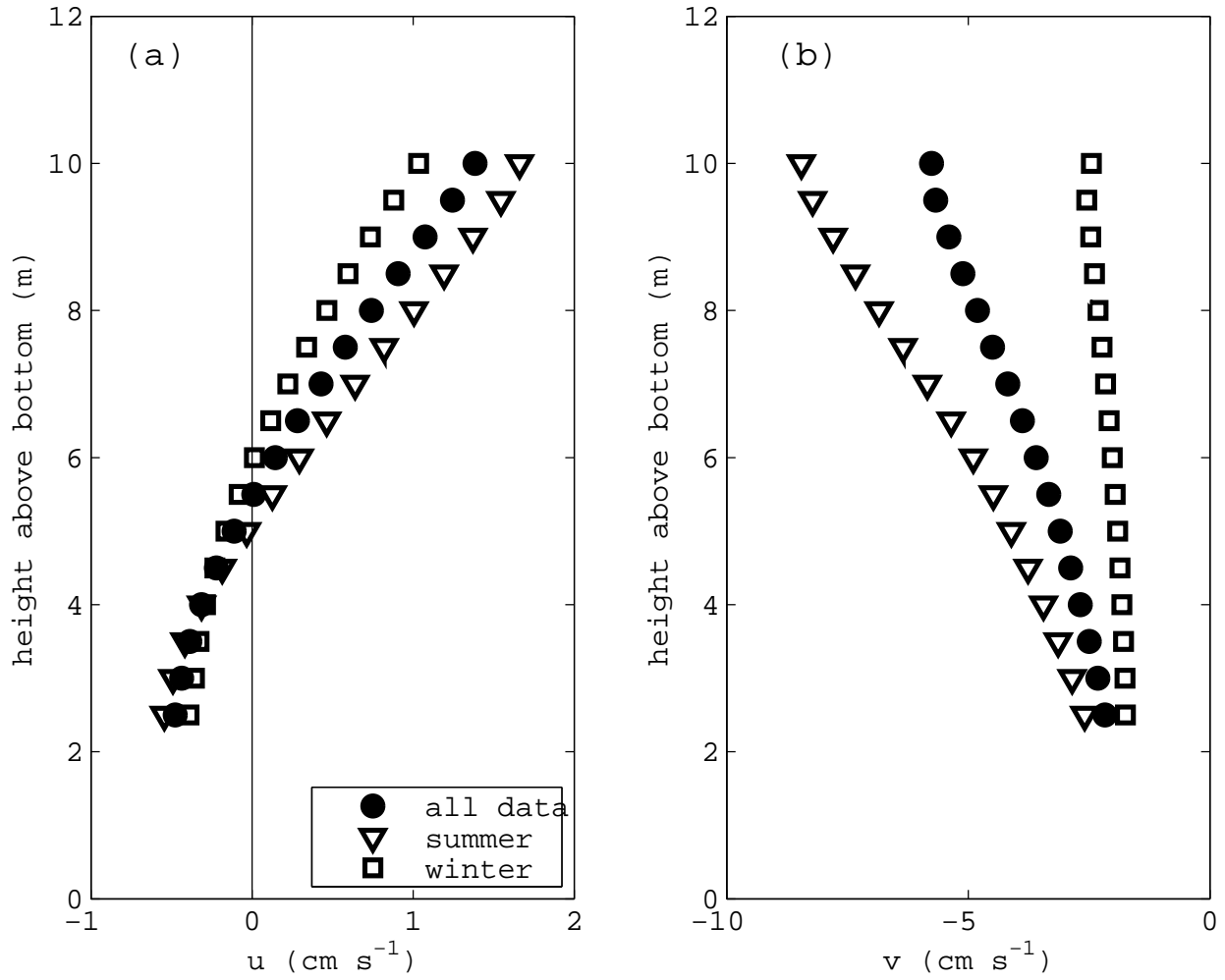
Figure 9: Average offshore flow profiles from MVCO for periods when $1 \text{ m} < H_{sig} < 2 \text{ m}$, and the wind stress was either offshore ($0.1 \text{ N m}^{-2} < \tau^{sx} < 0.2 \text{ N m}^{-2}$), onshore ($-0.2 \text{ N m}^{-2} < \tau^{sx} < -0.1 \text{ N m}^{-2}$), or weak ($|\boldsymbol{\tau}^s| < 0.03 \text{ N m}^{-2}$).

Figure 10: Average (a) cross-shelf u and (b) along-shelf v velocity profiles from MVCO for periods when the waves are small ($H_{sig} < 0.75$ m) and the wind stress is weak ($|\boldsymbol{\tau}^s| <$ 0.03 N m^{-2}), for all data, summer (April–September), and winter (October–March).

Figure 11: Average (a) cross-shelf u and (b) along-shelf v velocity profiles from MVCO for different ranges of H_{sig} during periods when the wind stress magnitude was small ($|\boldsymbol{\tau}^s| <$ 0.03 N m^{-2}) and corresponding model profiles (dashed lines) estimated using the average wave characteristics for each range of H_{sig} and a constant eddy viscosity of $A = 10^{-5}$ m^2 s^{-1}. Observed profiles for $H_{sig} < 0.75$ m are zero because the weak wind and small wave mean profile (Fig. 10) has been subtracted from all profiles. Standard errors of the means for the observed profiles are 0.1 cm s^{-1} for $0 < H_{sig} < 0.75$ and $0.75 < H_{sig} < 1.5$, 0.4 cm s^{-1} for $1.5 < H_{sig} < 2.25$, and 1.6 cm s^{-1} for $2.25 < H_{sig} < 3.5$. The reduced offshore currents in the top bin (height 10 m) may be due to contamination by surface reflections from the side-lobes of the ADCP acoustic pulses during large waves because of the reduced water depth under the wave troughs.
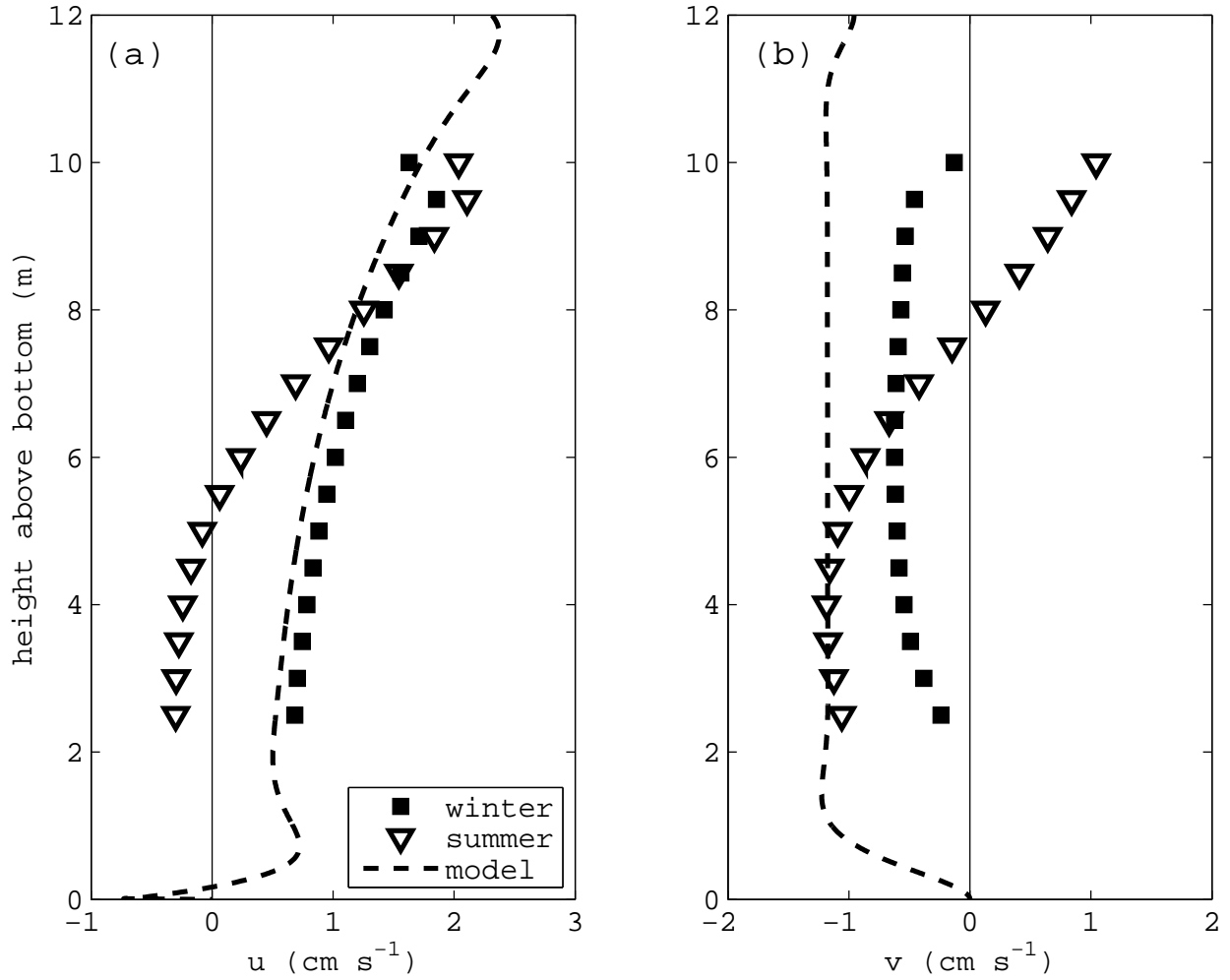
Figure 12: Average (a) cross-shelf u and (b) along-shelf v velocity profiles from MVCO for $1\,\mathrm{m} < H_{sig} < 2\,\mathrm{m}$ and $|\boldsymbol{\tau}^s| < 0.03\,\mathrm{N\,m^{-2}}$ during winter (October–March) and summer (April–September) and from the model for $A = 10^{-5}\,\mathrm{m^2\,s^{-1}}$ using the average wave characteristics for the selected observations. Only the average model profile is shown because the summer and winter model profiles are similar since the average wave characteristics are essentially the same. Standard errors of the means are $0.3\,\mathrm{cm\,s^{-1}}$ for the winter profile and $0.5\,\mathrm{cm\,s^{-1}}$ for the summer profile.
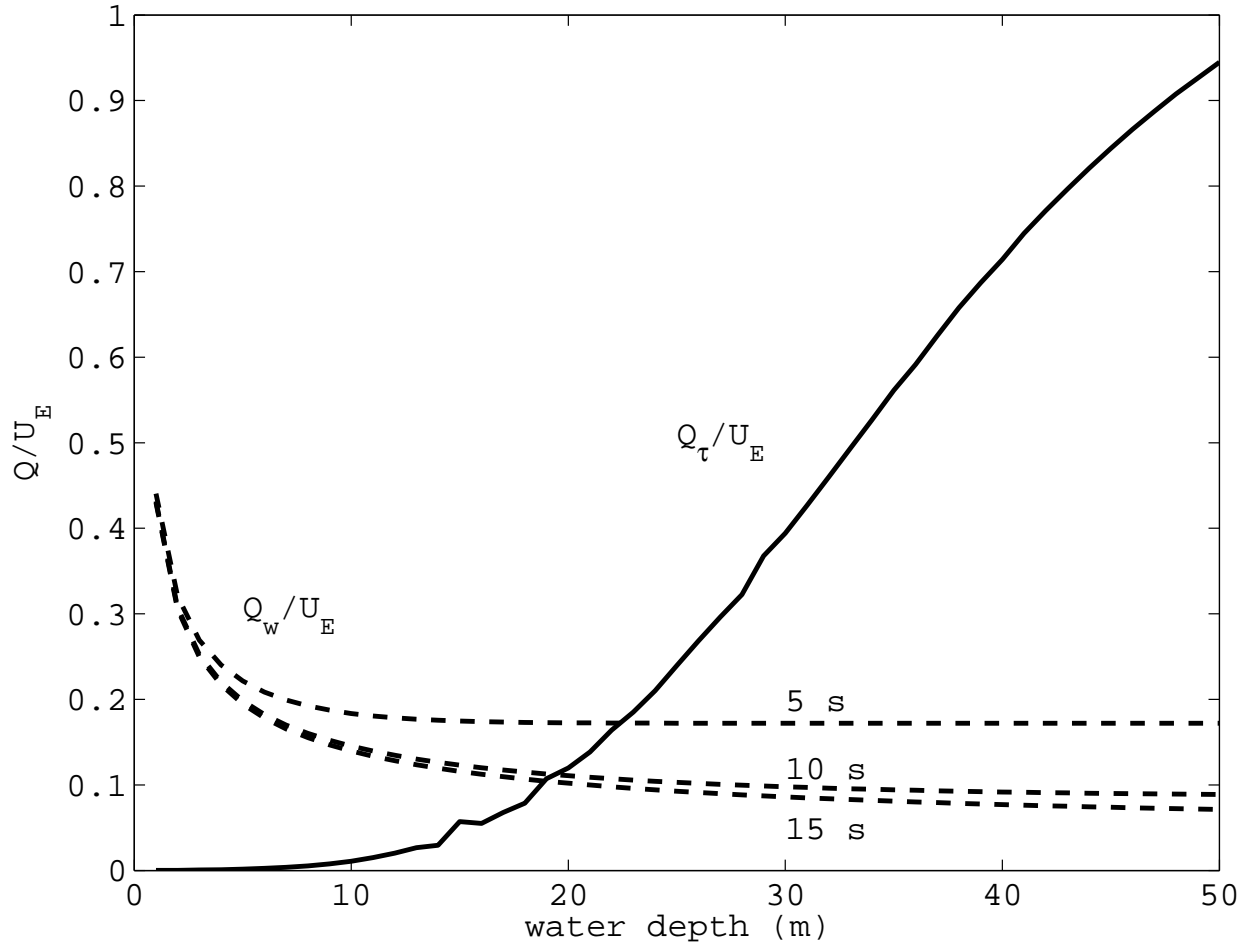
Figure 13: The wave-driven transport (Q_w) normalized by the Ekman transport (U_E) as a function of water depth for wave periods of 5, 10, and 15 s estimated from (14) assuming $H_{sig}^2/\tau^{sy} = 25$ m^4 N^{-1} (dashed lines). The solid line shows the normalized cross-shelf transport (Q_τ) driven by an along-shelf wind stress $(\tau^{sy} = 0.1$ N m$^{-2})$ as a function of water depth from a two-dimensional model (no along-shelf variation) with an unstratified turbulent eddy viscosity that increases linearly from zero at each boundary over 10% of the boundary layer thickness and is constant in the interior (see Lentz 1995).
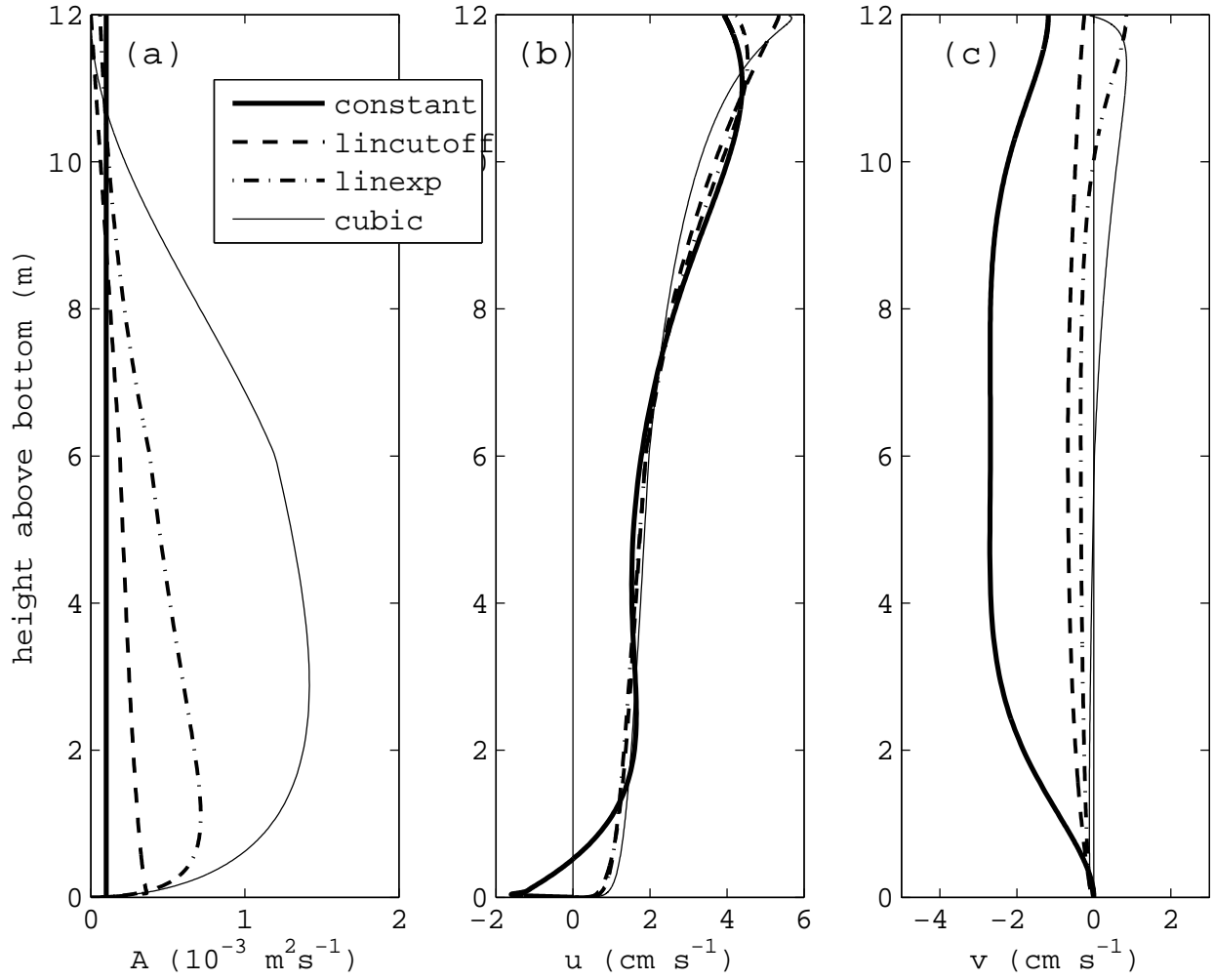
Figure 14: Profiles of (a) eddy viscosity A, (b) cross-shelf velocity u and (c) along-shelf velocity v from the numerical model for $H_{sig} = 2$ m, wave period of 7 s, water depth of 12 m, and bottom roughness of $z_o = 10^{-3}$ m.
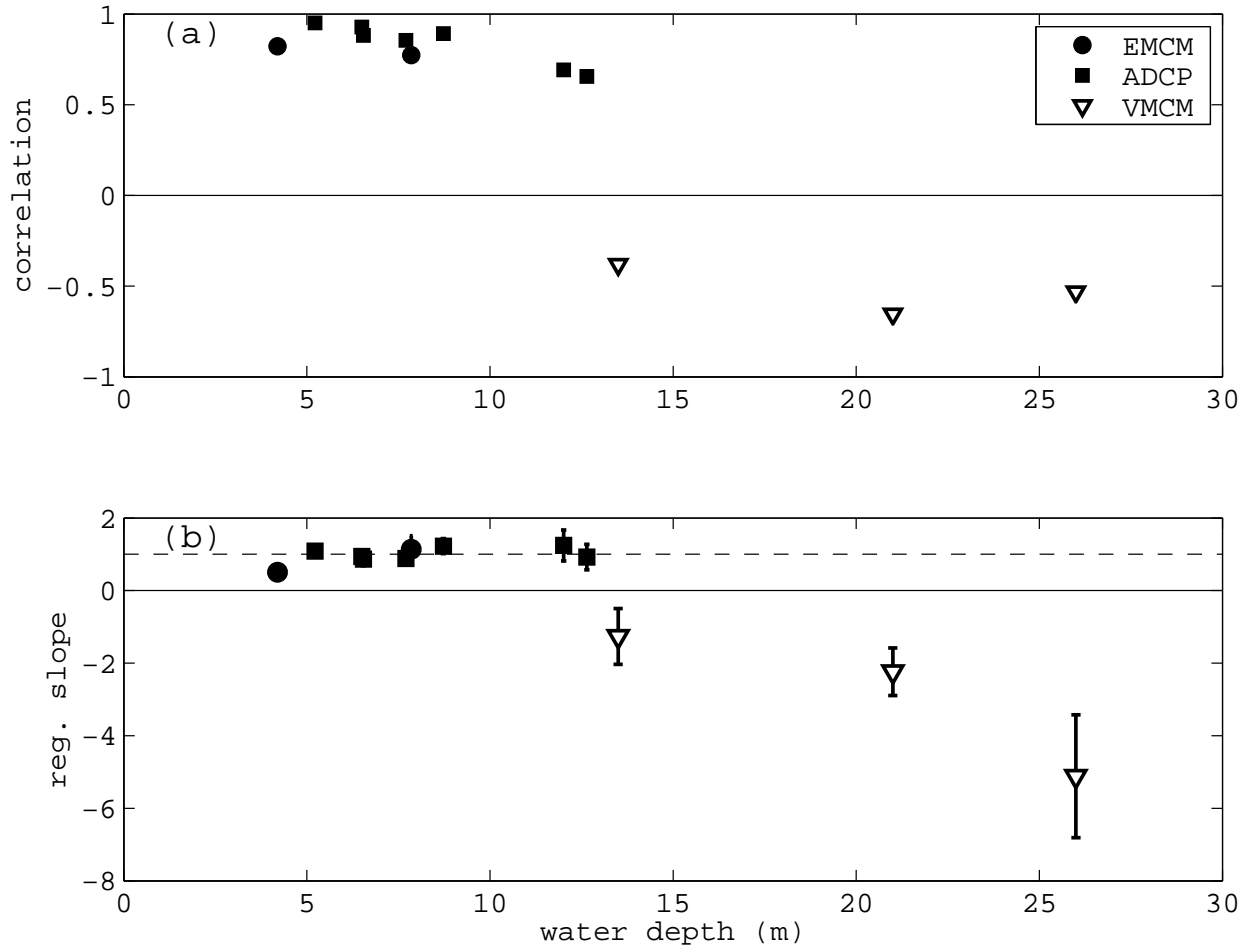
Figure 15: The (a) correlation and (b) regression slope a from linear regressions of the form $u_{da} = au_w + b$ for electromagnetic current meters (EMCM) and vector-measuring current meters (VMCM) deployed in 1994 on the North Carolina shelf and acoustic Doppler current profilers (ADCP) deployed at the same site in 1997. The error bars in (b) correspond to the 95% confidence intervals on the regression slope estimates. The negative correlations and regression slopes for the VMCMs are probably due to bias errors caused by inaccurate mechanical averaging of wave velocities.